Measurement of the B^+ production cross section in $p\bar{p}$ collisions at $\sqrt{s} = 1960$ GeV

A. Abulencia,[24] J. Adelman,[13] T. Affolder,[10] T. Akimoto,[56] M.G. Albrow,[17] D. Ambrose,[17] S. Amerio,[44] D. Amidei,[35] A. Anastassov,[53] K. Anikeev,[17] A. Annovi,[19] J. Antos,[14] M. Aoki,[56] G. Apollinari,[17] J.-F. Arguin,[34] T. Arisawa,[58] A. Artikov,[15] W. Ashmanskas,[17] A. Attal,[8] F. Azfar,[43] P. Azzi-Bacchetta,[44] P. Azzurri,[47] N. Bacchetta,[44] W. Badgett,[17] A. Barbaro-Galtieri,[29] V.E. Barnes,[49] B.A. Barnett,[25] S. Baroiant,[7] V. Bartsch,[31] G. Bauer,[33] F. Bedeschi,[47] S. Behari,[25] S. Belforte,[55] G. Bellettini,[47] J. Bellinger,[60] A. Belloni,[33] D. Benjamin,[16] A. Beretvas,[17] J. Beringer,[29] T. Berry,[30] A. Bhatti,[51] M. Binkley,[17] D. Bisello,[44] R.E. Blair,[2] C. Blocker,[6] B. Blumenfeld,[25] A. Bocci,[16] A. Bodek,[50] V. Boisvert,[50] G. Bolla,[49] A. Bolshov,[33] D. Bortoletto,[49] J. Boudreau,[48] A. Boveia,[10] B. Brau,[10] L. Brigliadori,[5] C. Bromberg,[36] E. Brubaker,[13] J. Budagov,[15] H.S. Budd,[50] S. Budd,[24] S. Budroni,[47] K. Burkett,[17] G. Busetto,[44] P. Bussey,[21] K. L. Byrum,[2] S. Cabrera[o],[16] M. Campanelli,[20] M. Campbell,[35] F. Canelli,[17] A. Canepa,[49] S. Carillo[i],[18] D. Carlsmith,[60] R. Carosi,[47] M. Casarsa,[55] A. Castro,[5] P. Catastini,[47] D. Cauz,[55] M. Cavalli-Sforza,[3] A. Cerri,[29] L. Cerrito[m],[43] S.H. Chang,[28] Y.C. Chen,[1] M. Chertok,[7] G. Chiarelli,[47] G. Chlachidze,[15] F. Chlebana,[17] I. Cho,[28] K. Cho,[28] D. Chokheli,[15] J.P. Chou,[22] G. Choudalakis,[33] S.H. Chuang,[60] K. Chung,[12] W.H. Chung,[60] Y.S. Chung,[50] M. Ciljak,[47] C.I. Ciobanu,[24] M.A. Ciocci,[47] A. Clark,[20] D. Clark,[6] M. Coca,[16] G. Compostella,[44] M.E. Convery,[51] J. Conway,[7] B. Cooper,[36] K. Copic,[35] M. Cordelli,[19] G. Cortiana,[44] F. Crescioli,[47] C. Cuenca Almenar,[7] J. Cuevas[l],[11] R. Culbertson,[17] J.C. Cully,[35] D. Cyr,[60] S. DaRonco,[44] M. Datta,[17] S. D'Auria,[21] T. Davies,[21] M. D'Onofrio,[3] D. Dagenhart,[6] P. de Barbaro,[50] S. De Cecco,[52] A. Deisher,[29] G. De Lentdecker[c],[50] M. Dell'Orso,[47] F. Delli Paoli,[44] L. Demortier,[51] J. Deng,[16] M. Deninno,[5] D. De Pedis,[52] P.F. Derwent,[17] G.P. Di Giovanni,[45] C. Dionisi,[52] B. Di Ruzza,[55] J.R. Dittmann,[4] P. DiTuro,[53] C. Dörr,[26] S. Donati,[47] M. Donega,[20] P. Dong,[8] J. Donini,[44] T. Dorigo,[44] S. Dube,[53] J. Efron,[40] R. Erbacher,[7] D. Errede,[24] S. Errede,[24] R. Eusebi,[17] H.C. Fang,[29] S. Farrington,[30] I. Fedorko,[47] W.T. Fedorko,[13] R.G. Feild,[61] M. Feindt,[26] J.P. Fernandez,[32] R. Field,[18] G. Flanagan,[49] A. Foland,[22]

S. Forrester,[7] G.W. Foster,[17] M. Franklin,[22] J.C. Freeman,[29] I. Furic,[13] M. Gallinaro,[51]
J. Galyardt,[12] J.E. Garcia,[47] F. Garberson,[10] A.F. Garfinkel,[49] C. Gay,[61] H. Gerberich,[24]
D. Gerdes,[35] S. Giagu,[52] P. Giannetti,[47] A. Gibson,[29] K. Gibson,[48] J.L. Gimmell,[50]
C. Ginsburg,[17] N. Giokaris[a],[15] M. Giordani,[55] P. Giromini,[19] M. Giunta,[47] G. Giurgiu,[12]
V. Glagolev,[15] D. Glenzinski,[17] M. Gold,[38] N. Goldschmidt,[18] J. Goldstein[b],[43]
A. Golossanov,[17] G. Gomez,[11] G. Gomez-Ceballos,[11] M. Goncharov,[54] O. González,[32]
I. Gorelov,[38] A.T. Goshaw,[16] K. Goulianos,[51] A. Gresele,[44] M. Griffiths,[30] S. Grinstein,[22]
C. Grosso-Pilcher,[13] R.C. Group,[18] U. Grundler,[24] J. Guimaraes da Costa,[22]
Z. Gunay-Unalan,[36] C. Haber,[29] K. Hahn,[33] S.R. Hahn,[17] E. Halkiadakis,[53] A. Hamilton,[34]
B.-Y. Han,[50] J.Y. Han,[50] R. Handler,[60] F. Happacher,[19] K. Hara,[56] M. Hare,[57] S. Harper,[43]
R.F. Harr,[59] R.M. Harris,[17] M. Hartz,[48] K. Hatakeyama,[51] J. Hauser,[8] A. Heijboer,[46]
B. Heinemann,[30] J. Heinrich,[46] C. Henderson,[33] M. Herndon,[60] J. Heuser,[26] D. Hidas,[16]
C.S. Hill[b],[10] D. Hirschbuehl,[26] A. Hocker,[17] A. Holloway,[22] S. Hou,[1] M. Houlden,[30]
S.-C. Hsu,[9] B.T. Huffman,[43] R.E. Hughes,[40] U. Husemann,[61] J. Huston,[36] J. Incandela,[10]
G. Introzzi,[47] M. Iori,[52] Y. Ishizawa,[56] A. Ivanov,[7] B. Iyutin,[33] E. James,[17] D. Jang,[53]
B. Jayatilaka,[35] D. Jeans,[52] H. Jensen,[17] E.J. Jeon,[28] S. Jindariani,[18] M. Jones,[49]
K.K. Joo,[28] S.Y. Jun,[12] J.E. Jung,[28] T.R. Junk,[24] T. Kamon,[54] P.E. Karchin,[59] Y. Kato,[42]
Y. Kemp,[26] R. Kephart,[17] U. Kerzel,[26] V. Khotilovich,[54] B. Kilminster,[40] D.H. Kim,[28]
H.S. Kim,[28] J.E. Kim,[28] M.J. Kim,[12] S.B. Kim,[28] S.H. Kim,[56] Y.K. Kim,[13] N. Kimura,[56]
L. Kirsch,[6] S. Klimenko,[18] M. Klute,[33] B. Knuteson,[33] B.R. Ko,[16] K. Kondo,[58]
D.J. Kong,[28] J. Konigsberg,[18] A. Korytov,[18] A.V. Kotwal,[16] A. Kovalev,[46] A.C. Kraan,[46]
J. Kraus,[24] I. Kravchenko,[33] M. Kreps,[26] J. Kroll,[46] N. Krumnack,[4] M. Kruse,[16]
V. Krutelyov,[10] T. Kubo,[56] S. E. Kuhlmann,[2] T. Kuhr,[26] Y. Kusakabe,[58] S. Kwang,[13]
A.T. Laasanen,[49] S. Lai,[34] S. Lami,[47] S. Lammel,[17] M. Lancaster,[31] R.L. Lander,[7]
K. Lannon,[40] A. Lath,[53] G. Latino,[47] I. Lazzizzera,[44] T. LeCompte,[2] J. Lee,[50] J. Lee,[28]
Y.J. Lee,[28] S.W. Lee[n],[54] R. Lefèvre,[3] N. Leonardo,[33] S. Leone,[47] S. Levy,[13] J.D. Lewis,[17]
C. Lin,[61] C.S. Lin,[17] M. Lindgren,[17] E. Lipeles,[9] A. Lister,[7] D.O. Litvintsev,[17] T. Liu,[17]
N.S. Lockyer,[46] A. Loginov,[61] M. Loreti,[44] P. Loverre,[52] R.-S. Lu,[1] D. Lucchesi,[44]
P. Lujan,[29] P. Lukens,[17] G. Lungu,[18] L. Lyons,[43] J. Lys,[29] R. Lysak,[14] E. Lytken,[49]
P. Mack,[26] D. MacQueen,[34] R. Madrak,[17] K. Maeshima,[17] K. Makhoul,[33] T. Maki,[23]

P. Maksimovic,[25] S. Malde,[43] G. Manca,[30] F. Margaroli,[5] R. Marginean,[17] C. Marino,[26] C.P. Marino,[24] A. Martin,[61] M. Martin,[21] V. Martin[g],[21] M. Martínez,[3] T. Maruyama,[56] P. Mastrandrea,[52] T. Masubuchi,[56] H. Matsunaga,[56] M.E. Mattson,[59] R. Mazini,[34] P. Mazzanti,[5] K.S. McFarland,[50] P. McIntyre,[54] R. McNulty[f],[30] A. Mehta,[30] P. Mehtala,[23] S. Menzemer[h],[11] A. Menzione,[47] P. Merkel,[49] C. Mesropian,[51] A. Messina,[36] T. Miao,[17] N. Miladinovic,[6] J. Miles,[33] R. Miller,[36] C. Mills,[10] M. Milnik,[26] A. Mitra,[1] G. Mitselmakher,[18] A. Miyamoto,[27] S. Moed,[20] N. Moggi,[5] B. Mohr,[8] R. Moore,[17] M. Morello,[47] P. Movilla Fernandez,[29] J. Mülmenstädt,[29] A. Mukherjee,[17] Th. Muller,[26] R. Mumford,[25] P. Murat,[17] J. Nachtman,[17] A. Nagano,[56] J. Naganoma,[58] I. Nakano,[41] A. Napier,[57] V. Necula,[18] C. Neu,[46] M.S. Neubauer,[9] J. Nielsen,[29] T. Nigmanov,[48] L. Nodulman,[2] O. Norniella,[3] E. Nurse,[31] S.H. Oh,[16] Y.D. Oh,[28] I. Oksuzian,[18] T. Okusawa,[42] R. Oldeman,[30] R. Orava,[23] K. Osterberg,[23] C. Pagliarone,[47] E. Palencia,[11] V. Papadimitriou,[17] A.A. Paramonov,[13] B. Parks,[40] S. Pashapour,[34] J. Patrick,[17] G. Pauletta,[55] M. Paulini,[12] C. Paus,[33] D.E. Pellett,[7] A. Penzo,[55] T.J. Phillips,[16] G. Piacentino,[47] J. Piedra,[45] L. Pinera,[18] K. Pitts,[24] C. Plager,[8] L. Pondrom,[60] X. Portell,[3] O. Poukhov,[15] N. Pounder,[43] F. Prakoshyn,[15] A. Pronko,[17] J. Proudfoot,[2] F. Ptohos[e],[19] G. Punzi,[47] J. Pursley,[25] J. Rademacker[b],[43] A. Rahaman,[48] N. Ranjan,[49] S. Rappoccio,[22] B. Reisert,[17] V. Rekovic,[38] P. Renton,[43] M. Rescigno,[52] S. Richter,[26] F. Rimondi,[5] L. Ristori,[47] A. Robson,[21] T. Rodrigo,[11] E. Rogers,[24] S. Rolli,[57] R. Roser,[17] M. Rossi,[55] R. Rossin,[18] A. Ruiz,[11] J. Russ,[12] V. Rusu,[13] H. Saarikko,[23] S. Sabik,[34] A. Safonov,[54] W.K. Sakumoto,[50] G. Salamanna,[52] O. Saltó,[3] D. Saltzberg,[8] C. Sánchez,[3] L. Santi,[55] S. Sarkar,[52] L. Sartori,[47] K. Sato,[17] P. Savard,[34] A. Savoy-Navarro,[45] T. Scheidle,[26] P. Schlabach,[17] E.E. Schmidt,[17] M.P. Schmidt,[61] M. Schmitt,[39] T. Schwarz,[7] L. Scodellaro,[11] A.L. Scott,[10] A. Scribano,[47] F. Scuri,[47] A. Sedov,[49] S. Seidel,[38] Y. Seiya,[42] A. Semenov,[15] L. Sexton-Kennedy,[17] A. Sfyrla,[20] M.D. Shapiro,[29] T. Shears,[30] P.F. Shepard,[48] D. Sherman,[22] M. Shimojima[k],[56] M. Shochet,[13] Y. Shon,[60] I. Shreyber,[37] A. Sidoti,[47] P. Sinervo,[34] A. Sisakyan,[15] J. Sjolin,[43] A.J. Slaughter,[17] J. Slaunwhite,[40] K. Sliwa,[57] J.R. Smith,[7] F.D. Snider,[17] R. Snihur,[34] M. Soderberg,[35] A. Soha,[7] S. Somalwar,[53] V. Sorin,[36] J. Spalding,[17] F. Spinella,[47] T. Spreitzer,[34] P. Squillacioti,[47] M. Stanitzki,[61] A. Staveris-Polykalas,[47] R. St. Denis,[21] B. Stelzer,[8] O. Stelzer-Chilton,[43]

D. Stentz,[39] J. Strologas,[38] D. Stuart,[10] J.S. Suh,[28] A. Sukhanov,[18] H. Sun,[57] T. Suzuki,[56] A. Taffard,[24] R. Takashima,[41] Y. Takeuchi,[56] K. Takikawa,[56] M. Tanaka,[2] R. Tanaka,[41] M. Tecchio,[35] P.K. Teng,[1] K. Terashi,[51] J. Thom[d],[17] A.S. Thompson,[21] E. Thomson,[46] P. Tipton,[61] V. Tiwari,[12] S. Tkaczyk,[17] D. Toback,[54] S. Tokar,[14] K. Tollefson,[36] T. Tomura,[56] D. Tonelli,[47] S. Torre,[19] D. Torretta,[17] S. Tourneur,[45] W. Trischuk,[34] R. Tsuchiya,[58] S. Tsuno,[41] N. Turini,[47] F. Ukegawa,[56] T. Unverhau,[21] S. Uozumi,[56] D. Usynin,[46] S. Vallecorsa,[20] N. van Remortel,[23] A. Varganov,[35] E. Vataga,[38] F. Vázquez[i],[18] G. Velev,[17] G. Veramendi,[24] V. Veszpremi,[49] R. Vidal,[17] I. Vila,[11] R. Vilar,[11] T. Vine,[31] I. Vollrath,[34] I. Volobouev[n],[29] G. Volpi,[47] F. Würthwein,[9] P. Wagner,[54] R.G. Wagner,[2] R.L. Wagner,[17] J. Wagner,[26] W. Wagner,[26] R. Wallny,[8] S.M. Wang,[1] A. Warburton,[34] S. Waschke,[21] D. Waters,[31] B. Whitehouse,[57] D. Whiteson,[46] A.B. Wicklund,[2] E. Wicklund,[17] G. Williams,[34] H.H. Williams,[46] P. Wilson,[17] B.L. Winer,[40] P. Wittich[d],[17] S. Wolbers,[17] C. Wolfe,[13] T. Wright,[35] X. Wu,[20] S.M. Wynne,[30] A. Yagil,[17] K. Yamamoto,[42] J. Yamaoka,[53] T. Yamashita,[41] C. Yang,[61] U.K. Yang[j],[13] Y.C. Yang,[28] W.M. Yao,[29] G.P. Yeh,[17] J. Yoh,[17] K. Yorita,[13] T. Yoshida,[42] G.B. Yu,[50] I. Yu,[28] S.S. Yu,[17] J.C. Yun,[17] L. Zanello,[52] A. Zanetti,[55] I. Zaw,[22] X. Zhang,[24] J. Zhou,[53] and S. Zucchelli[5]

(CDF Collaboration*)

[1]*Institute of Physics, Academia Sinica, Taipei, Taiwan 11529, Republic of China*

[2]*Argonne National Laboratory, Argonne, Illinois 60439*

[3]*Institut de Fisica d'Altes Energies, Universitat Autonoma de Barcelona, E-08193, Bellaterra (Barcelona), Spain*

[4]*Baylor University, Waco, Texas 76798*

[5]*Istituto Nazionale di Fisica Nucleare, University of Bologna, I-40127 Bologna, Italy*

* With visitors from [a]University of Athens, [b]University of Bristol, [c]University Libre de Bruxelles, [d]Cornell University, [e]University of Cyprus, [f]University of Dublin, [g]University of Edinburgh, [h]University of Heidelberg, [i]Universidad Iberoamericana, [j]University of Manchester, [k]Nagasaki Institute of Applied Science, [l]University de Oviedo, [m]University of London, Queen Mary and Westfield College, [n]Texas Tech University, [o]IFIC(CSIC-Universitat de Valencia),

[6]Brandeis University, Waltham, Massachusetts 02254
[7]University of California, Davis, Davis, California 95616
[8]University of California, Los Angeles, Los Angeles, California 90024
[9]University of California, San Diego, La Jolla, California 92093
[10]University of California, Santa Barbara, Santa Barbara, California 93106
[11]Instituto de Fisica de Cantabria, CSIC-University of Cantabria, 39005 Santander, Spain
[12]Carnegie Mellon University, Pittsburgh, PA 15213
[13]Enrico Fermi Institute, University of Chicago, Chicago, Illinois 60637
[14]Comenius University, 842 48 Bratislava,
Slovakia; Institute of Experimental Physics, 040 01 Kosice, Slovakia
[15]Joint Institute for Nuclear Research, RU-141980 Dubna, Russia
[16]Duke University, Durham, North Carolina 27708
[17]Fermi National Accelerator Laboratory, Batavia, Illinois 60510
[18]University of Florida, Gainesville, Florida 32611
[19]Laboratori Nazionali di Frascati, Istituto Nazionale
di Fisica Nucleare, I-00044 Frascati, Italy
[20]University of Geneva, CH-1211 Geneva 4, Switzerland
[21]Glasgow University, Glasgow G12 8QQ, United Kingdom
[22]Harvard University, Cambridge, Massachusetts 02138
[23]Division of High Energy Physics, Department of Physics,
University of Helsinki and Helsinki Institute of Physics, FIN-00014, Helsinki, Finland
[24]University of Illinois, Urbana, Illinois 61801
[25]The Johns Hopkins University, Baltimore, Maryland 21218
[26]Institut für Experimentelle Kernphysik,
Universität Karlsruhe, 76128 Karlsruhe, Germany
[27]High Energy Accelerator Research Organization (KEK), Tsukuba, Ibaraki 305, Japan
[28]Center for High Energy Physics: Kyungpook National University,
Taegu 702-701, Korea; Seoul National University, Seoul 151-742,
Korea; and SungKyunKwan University, Suwon 440-746, Korea
[29]Ernest Orlando Lawrence Berkeley National Laboratory, Berkeley, California 94720
[30]University of Liverpool, Liverpool L69 7ZE, United Kingdom
[31]University College London, London WC1E 6BT, United Kingdom

[32]Centro de Investigaciones Energeticas
Medioambientales y Tecnologicas, E-28040 Madrid, Spain
[33]Massachusetts Institute of Technology, Cambridge, Massachusetts 02139
[34]Institute of Particle Physics: McGill University, Montréal,
Canada H3A 2T8; and University of Toronto, Toronto, Canada M5S 1A7
[35]University of Michigan, Ann Arbor, Michigan 48109
[36]Michigan State University, East Lansing, Michigan 48824
[37]Institution for Theoretical and Experimental Physics, ITEP, Moscow 117259, Russia
[38]University of New Mexico, Albuquerque, New Mexico 87131
[39]Northwestern University, Evanston, Illinois 60208
[40]The Ohio State University, Columbus, Ohio 43210
[41]Okayama University, Okayama 700-8530, Japan
[42]Osaka City University, Osaka 588, Japan
[43]University of Oxford, Oxford OX1 3RH, United Kingdom
[44]University of Padova, Istituto Nazionale di Fisica Nucleare,
Sezione di Padova-Trento, I-35131 Padova, Italy
[45]LPNHE, Universite Pierre et Marie
Curie/IN2P3-CNRS, UMR7585, Paris, F-75252 France
[46]University of Pennsylvania, Philadelphia, Pennsylvania 19104
[47]Istituto Nazionale di Fisica Nucleare Pisa, Universities of Pisa,
Siena and Scuola Normale Superiore, I-56127 Pisa, Italy
[48]University of Pittsburgh, Pittsburgh, Pennsylvania 15260
[49]Purdue University, West Lafayette, Indiana 47907
[50]University of Rochester, Rochester, New York 14627
[51]The Rockefeller University, New York, New York 10021
[52]Istituto Nazionale di Fisica Nucleare, Sezione di Roma 1,
University of Rome "La Sapienza," I-00185 Roma, Italy
[53]Rutgers University, Piscataway, New Jersey 08855
[54]Texas A&M University, College Station, Texas 77843
[55]Istituto Nazionale di Fisica Nucleare, University of Trieste/ Udine, Italy
[56]University of Tsukuba, Tsukuba, Ibaraki 305, Japan
[57]Tufts University, Medford, Massachusetts 02155

[58]*Waseda University, Tokyo 169, Japan*

[59]*Wayne State University, Detroit, Michigan 48201*

[60]*University of Wisconsin, Madison, Wisconsin 53706*

[61]*Yale University, New Haven, Connecticut 06520*

Abstract

We present a new measurement of the B^+ meson differential cross section $d\sigma/dp_T$ at $\sqrt{s} = 1960$ GeV. The data correspond to an integrated luminosity of 739 pb^{-1} collected with the upgraded CDF detector (CDF II) at the Fermilab Tevatron collider. B^+ candidates are reconstructed through the decay $B^+ \to J/\psi\ K^+$, with $J/\psi \to \mu^+\ \mu^-$. The integrated cross section for producing B^+ mesons with $p_T \geq 6$ GeV/c and $|y| \leq 1$ is measured to be 2.78 ± 0.24 μb.

PACS numbers: 13.85.Ni, 12.38.Qk, 13.25.Hw, 14.40.Nd

I. INTRODUCTION

Measurements of the bottom quark production cross section at the Tevatron collider probe the ability of perturbative QCD to predict absolute rates in hadronic collisions. At the perturbative level, calculations of the hard scattering cross sections have been carried out at next-to-leading order (NLO) [1] and also implemented with logarithmic p_T^b/m_b [1] corrections evaluated to next-to-leading logarithmic accuracy (NLL) [2]. In both cases, these QCD predictions are affected by large theoretical uncertainties such as the dependence on the choice of the renormalization and factorization scales and the b-quark mass [3, 4]. Accurate measurements could help in improving the theoretical prediction. Unfortunately, as noted in Ref. [5], measurements of the b-quark cross section at the Tevatron appear to be inconsistent among themselves. Reference [5] uses the prediction of a NLO calculation [1] implemented with a non-perturbative model for the b-quark fragmentation [2] in order to compare all measurements performed at the Tevatron. This calculation predicts $\sigma(p_T^{B^+} \geq 6$ GeV/c, $|y|^{B^+} \leq 1) = 0.9$ μb. Previous measurements [9, 10] performed by the CDF collaboration at $\sqrt{s} = 1.8$ TeV yield $\sigma(p_T^{B^+} \geq 6$ GeV/c, $|y|^{B^+} \leq 1) = 2.66 \pm 0.61$ and 3.6 ± 0.6 μb, respectively. The ratios of these measurements to the NLO prediction are (2.9 ± 0.67) and (4.0 ± 0.6), respectively. In contrast, the ratios of the CDF and DØ measurements of the b cross section, that are not based upon the detection of J/ψ mesons [11–15], to the same theoretical prediction have an appreciably smaller average (2.2 with a 0.2 RMS deviation [5]). The cause of the inconsistency could be experimental difficulties inherent to each result or some underlying, and not yet appreciated, production of new physics. Therefore, it is of interest to clarify the experimental situation.

This paper presents a new measurement of the B^+ production cross section that uses fully reconstructed $B^\pm \to J/\psi\ K^\pm$ decays. We follow closely the experimental procedure used in Refs. [9, 10], but we simplify the analysis selection criteria in order to reduce systematic uncertainties. The B^+ production cross section is the ratio of the number of observed B^+ candidates to the product of the detector acceptance, integrated luminosity, and branching

[1] Mass (m_b) and transverse momentum (p_T^b) of the bottom quarks involved in the hard scattering.

[2] This calculation uses a b-quark mass of $m_b = 4.75$ GeV/c^2, renormalization and factorization scales $\mu_R = \mu_F = \sqrt{p_T^2 + m_b^2}$, the MRSD$_0$ [6] fit to the parton distribution functions (PDF), and a fragmentation fraction $f_u = 0.375$. The fragmentation model is based on the Peterson fragmentation function [7] with the ϵ parameter set to 0.006 according to fits to e^+e^- data [8].

fraction of the decay $B^+ \to J/\psi\, K^+$ with $J/\psi \to \mu^+\, \mu^-$. Section II describes the detector systems relevant to this analysis. The data collection, event selection, and $B^\pm$ reconstruction are described in Sec. III. In Sec. IV, we evaluate the detector acceptance and derive the total and differential B^+ cross section. Our conclusions are presented in Sec. V.

II. THE CDF II DETECTOR

CDF is a multipurpose detector, equipped with a charged particle spectrometer and a finely segmented calorimeter. In this section, we describe the detector components that are relevant to this analysis. The description of these subsystems can be found in Refs. [16–22]. Two devices inside the 1.4 T solenoid are used for measuring the momentum of charged particles: the silicon vertex detector (SVX II) and the central tracking chamber (COT). The SVX II consists of double-sided microstrip sensors arranged in five cylindrical shells with radii between 2.5 and 10.6 cm. The detector is divided into three contiguous five-layer sections along the beam direction for a total z coverage [3] of 90 cm. The COT is a cylindrical drift chamber containing 96 sense wire layers grouped into eight alternating superlayers of axial and stereo wires. Its active volume covers $|z| \leq 155$ cm and 40 to 140 cm in radius. The central muon detector (CMU) is located around the central electromagnetic and hadronic calorimeters, which have a thickness of 5.5 interaction lengths at normal incidence.

The CMU detector covers a nominal pseudorapidity range $|\eta| \leq 0.63$ relative to the center of the detector, and is segmented into two barrels of 24 modules, each covering 15° in ϕ. Every module is further segmented into three submodules, each covering 4.2° in ϕ and consisting of four layers of drift chambers. The smallest drift unit, called a stack, covers a 1.2° angle in ϕ. Adjacent pairs of stacks are combined together into a tower. A track segment (hits in two out of four layers of a stack) detected in a tower is referred to as a CMU stub. A second set of muon drift chambers (CMP) is located behind an additional steel absorber of 3.3 interaction lengths. Muons which produce a stub in both CMU and CMP systems are called CMUP muons.

[3] In the CDF coordinate system, θ and ϕ are the polar and azimuthal angles of a track, respectively, defined with respect to the proton beam direction, z. The pseudorapidity η is defined as $-\log\ \tan(\theta/2)$. The transverse momentum of a particle is $p_T = P\ \sin(\theta)$. The rapidity is defined as $y = 1/2 \cdot \log((E+p_z)/(E-p_z))$, where E and p_z are the energy and longitudinal momentum of the particle associated with the track.

The luminosity is measured using gaseous Cherenkov counters (CLC) that monitor the rate of inelastic $p\bar{p}$ collisions. The inelastic $p\bar{p}$ cross section at $\sqrt{s} = 1960$ GeV is scaled from measurements at $\sqrt{s} = 1800$ GeV using the calculations in Ref. [23]. The integrated luminosity is determined with a 6% systematic accuracy [24].

CDF uses a three-level trigger system. At Level 1 (L1), data from every beam crossing are stored in a pipeline capable of buffering data from 42 beam crossings. The L1 trigger either rejects events or copies them into one of the four Level 2 (L2) buffers. Events that pass the L1 and L2 selection criteria are sent to the Level 3 (L3) trigger, a cluster of computers running speed-optimized reconstruction code.

For this study, we select events with two muon candidates identified by the L1 and L2 triggers. The L1 trigger uses tracks with $p_T \geq 1.5$ GeV/c found by a fast track processor (XFT). The XFT examines COT hits from four axial superlayers and provides $r-\phi$ information. The XFT finds tracks with $p_T \geq 1.5$ GeV/c in azimuthal sections of 1.25°. The XFT passes the tracks to a set of extrapolation units that determines the CMU towers in which a CMU stub should be found if the track is a muon. If a stub is found, a L1 CMU primitive is generated. The L1 dimuon trigger requires at least two CMU primitives, separated by at least two CMU towers. At L1, there is no requirement that muons have opposite charge. During the data-taking period in which the dimuon sample used for this analysis was collected, the Tevatron luminosity has increased from 1 to 100×10^{30} cm^{-2} s^{-1}. Accordingly, the L2 trigger, that started with no additional requirement, has incrementally required dimuons with opposite charge, opening azimuthal angle $\delta\phi \leq 120^\circ$, and $p_T \geq 2$ GeV/c. All these trigger requirements are mimicked by the detector simulation on a run-by-run basis. At L3, muons are required to have opposite charge, invariant mass in the window $2.7-4.0$ GeV/c^2, and $|\delta z_0| \leq 5$ cm, where z_0 is the z coordinate of the muon track at its point of closest approach to the beam line in the $r-\phi$ plane. These requirements define the $J/\psi \to \mu^+\mu^-$ trigger.

We use two additional triggers in order to verify the detector simulation. The first trigger (CMUPp_T4) selects events with at least one L1 and one L2 CMUP primitive with $p_T \geq 4$ GeV/c, and an additional muon found by the L3 algorithms. Events collected with this trigger are used to measure the muon trigger efficiency. The second trigger (μ–SVT) requires a L1 CMUP primitive with $p_T \geq 4$ GeV/c accompanied by a L2 requirement of an additional XFT track with $p_T \geq 2$ GeV/c and displaced from the interaction point.

These events are used to verify the muon detector acceptance and the muon reconstruction efficiency.

III. DATA SELECTION AND $B^{\pm}$ RECONSTRUCTION

We search for $B^{\pm} \to J/\psi K^{\pm}$ candidates in the data set selected by the $J/\psi \to \mu^+\mu^-$ trigger. Events are reconstructed off-line taking advantage of more refined calibration constants and reconstruction algorithms.

The transverse momentum resolution of tracks reconstructed using COT hits is $\sigma(p_T)/p_T^2 \simeq 0.0017$ $[\mathrm{GeV/c}]^{-1}$. COT tracks are extrapolated into the SVX II detector and refitted adding hits consistent with the track extrapolation. Stubs reconstructed in the CMU detector are matched to tracks with $p_T \geq 1.3$ GeV/c. A track is identified as a CMU muon if $\Delta r\phi$, the distance in the $r-\phi$ plane between the track projected to the CMU chambers and a CMU stub, is less than 30 cm. We also require that muon-candidate stubs correspond to a L1 CMU primitive, and correct the muon momentum for energy losses in the detector.

We search for J/ψ candidates by using pairs of CMU muons with opposite charge, and $p_T \geq 2$ GeV/c (this requirement avoids the region of rapidly changing efficiency around the trigger threshold). The invariant mass of a muon pair is evaluated by constraining the two muon tracks to originate from a common point in three-dimensional space (vertex constraint) in order to improve the mass resolution. All muon pairs with invariant mass in the range $3.05 - 3.15$ GeV/c^2 are considered to be J/ψ candidates.

If a J/ψ candidate is found, we search for $B^{\pm}$ mesons by considering all remaining charged particle tracks in the event as possible kaon candidates. As in previous measurements [9, 10], we select tracks with $p_T \geq 1.25$ GeV/c and with $|\delta z_0| \leq 1.5$ cm with respect to the z_0 position of the J/ψ candidate. We require that kaon-candidate tracks have at least 10 hits in both COT axial and stereo superlayers. This limits the pseudorapidity acceptance to $|\eta| \leq 1.3$. The invariant mass of the μ^+ μ^- $K^{\pm}$ system is evaluated constraining the corresponding tracks to have a common origin while the μ^+ μ^- invariant mass is constrained to the value of 3.0969 GeV/c^2 [25]. As in Refs. [9, 10], we select $B^{\pm}$ candidates with $p_T \geq 6$ GeV/c. From the pseudorapidity acceptance of CMU muons ($|\eta| \leq 0.8$) and the p_T cuts on the $\mu^{\pm}$ and $B^{\pm}$ transverse momenta, it follows that: (1) no kaon from $B^{\pm}$ decays is emitted at $|\eta| \geq 1.3$;

(2) the reconstructed $B^{\pm}$ candidates have rapidity $|y| \leq 1$.

In contrast with the analyses in Refs. [9, 10], we do not require the proper decay length of the $B^{\pm}$ candidates to be larger than 100 μm. By doing so, we avoid two large sources of systematic uncertainty: (1) the simulated efficiency of the SVX II detector; (2) the dependence of the decay length distribution on the simulated SVX II resolution and $B^{\pm}$ transverse momentum distribution. The invariant mass distribution of all $B^{\pm}$ candidates found in this study is shown in Fig. 1.

IV. DIFFERENTIAL CROSS SECTION

To measure the differential cross section, we divide the sample of $B^{\pm}$ candidates into five p_T bins: $6-9$, $9-12$, $12-15$, $15-25$, and ≥ 25 GeV/c [9, 10]. In each p_T bin, we fit the invariant mass distribution of the $B^{\pm}$ candidates with a binned maximum-likelihood method to determine the number of $B^{\pm}$ mesons. The fit likelihood uses a Gaussian function to model the $B^{\pm}$ signal. As in the previous measurements [9, 10], we use a first order polynomial to estimate the underlying combinatorial background. As shown by Fig. 1, the mass region above the $B^{\pm}$ meson signal is not affected by partially reconstructed $B^{\pm}$ decays and is quite well described by a straight line. We fit the data in the invariant mass range $5.18-5.39$ GeV/c^2. The lower limit is chosen to avoid the region populated by partially reconstructed $B^{\pm}$ decays. The width of the fitted mass range determines the statistical error of the background estimate. Since we have a much larger data set than previous measurements [9, 10], we can afford to fit the data in a smaller mass range in order to reduce the systematic uncertainty due to the background modeling.

The average of the $B^{\pm}$ mass values returned by the fits in the different p_T bins is 5.2790 GeV/c^2 with a 0.5 MeV/c^2 RMS deviation, in agreement with the PDG value [25]. In the fit used to determine the number of $B^{\pm}$ mesons, we fix the $B^{\pm}$ mass value to 5.279 GeV/c^2 [25]. The width of the Gaussian is a free fit parameter; the value of σ returned by the fit increases from 12.0 ± 0.4 to 20.0 ± 0.4 MeV/c^2 from the first to last p_T bin, in agreement with the simulation prediction. The fits are shown in Figs. 2 to 6. They return a signal of 2792 ± 186, 2373 ± 110, 1365 ± 66, 1390 ± 63, and 277 ± 44 $B^{\pm}$ mesons in the five p_T bins.

We have investigated possible systematic uncertainties in the fit results. We have studied

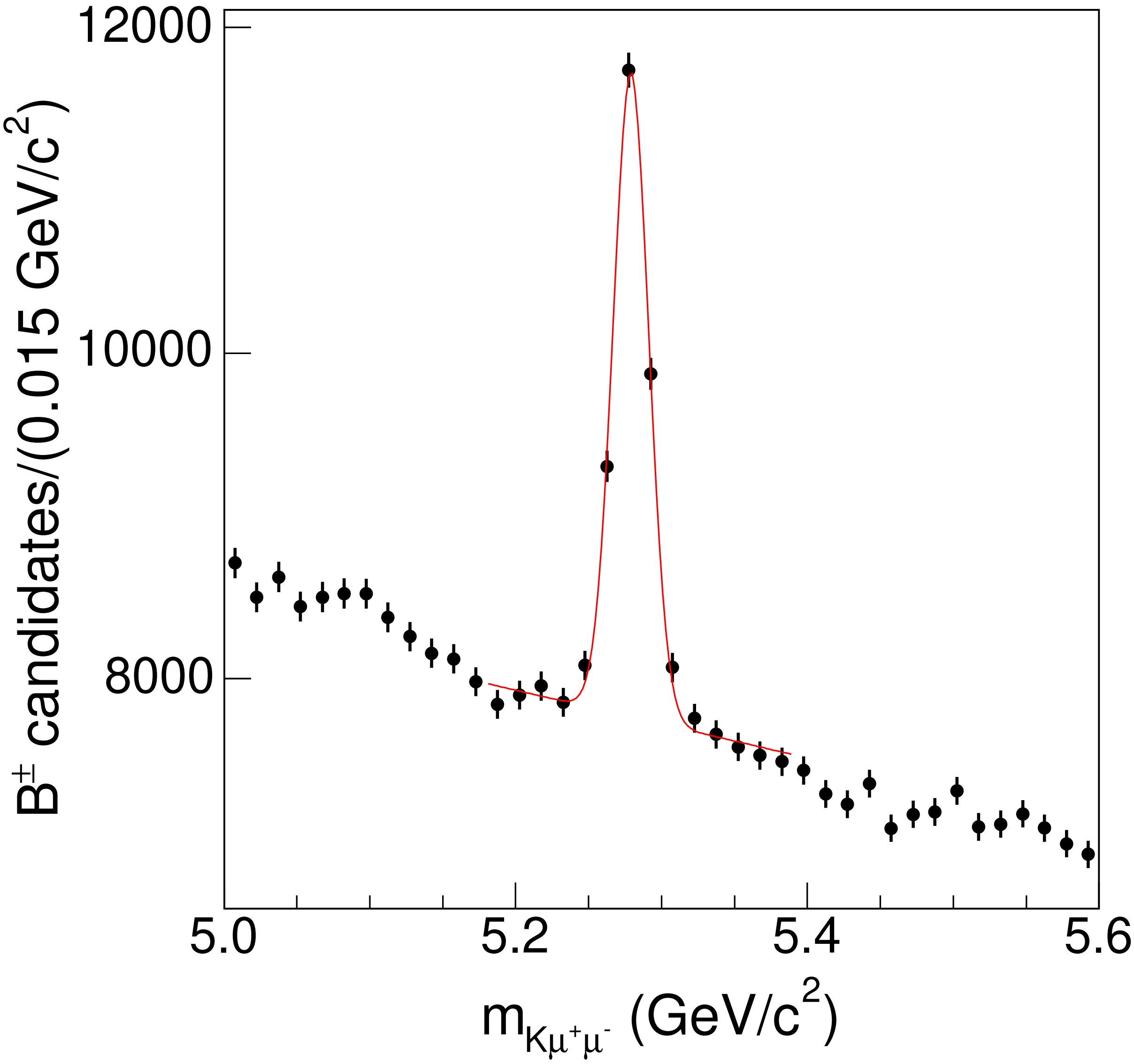

FIG. 1: Invariant mass distribution of all $B^{\pm}$ candidates. The line represents a fit to the data using a first order polynomial plus a Gaussian function in order to estimate the background and the $B^{\pm}$ signal, respectively.

the contribution of the $B \to J/\psi\ \pi$ decay mode, the branching fraction of which is $(4.9 \pm 0.6)\%$ of that of the $B \to J/\psi\ K$ decay mode [25]. As shown in Ref. [26], the invariant mass distribution of Cabibbo-suppressed B decays, reconstructed assuming that pions are kaons, is shifted into the mass region $5.28 - 5.44$ GeV/c^2, which partially overlaps with that of

TABLE I: Detector acceptance, $\mathcal{A}$, as a function of the $B^{\pm}$ p_T. The acceptance $\mathcal{A}_{\mathrm{corr}}$ includes corrections evaluated using the data. The average $< p_T >$ is the value at which the theoretical differential cross section [1] equals the integrated cross section in each momentum bin divided by the bin width.

p_T range (GeV/c)	$< p_T >$ (GeV/c)	$\mathcal{A}$ (%)	$\mathcal{A}_{\mathrm{corr}}$ (%)
$6-9$	7.37	1.545	1.780 ± 0.045
$9-12$	10.38	3.824	4.405 ± 0.111
$12-15$	13.39	5.966	6.872 ± 0.173
$15-25$	19.10	8.819	10.16 ± 0.25
≥ 25		12.516	14.42 ± 0.36

the $B \to J/\psi\ K$ decay mode. However, part of the Cabibbo-suppressed contribution is also used by the fit to predict the background under the $B \to J/\psi\ K$ signal with the effect of reducing its size. When adding the expected contribution of the Cabibbo-suppressed decays, the $B \to J/\psi\ K$ signal returned by the fit decreases by $(1 \pm 1)\%$. We have investigated other possible causes of systematic uncertainties in the B signal estimate. We have compared the results of our fit with those returned using an unbinned likelihood method. We have decreased the fitted mass range to $5.24 - 5.33$ GeV/c^2, and we have fitted the larger mass interval $5.18 - 5.60$ GeV/c^2. We have fitted the signal with two Gaussian functions in order to study detector resolution effects. The B signal returned by these fits does not vary by more than $\pm 1.5\%$. Therefore, we attribute an overall $\pm 2\%$ systematic uncertainty to the fit results.

A. Acceptances and Efficiencies

The detector acceptance is calculated with a Monte Carlo simulation based upon a NLO calculation [2]. The $B^{\pm}$ decay is modeled with the EVTGEN Monte Carlo program [27] that accounts for the J/ψ longitudinal polarization [28]. The detector response to particles produced by $B^{\pm}$ decays is modeled with the CDF II detector simulation that in turn is based on the GEANT Monte Carlo program [29]. The simulation includes the generation

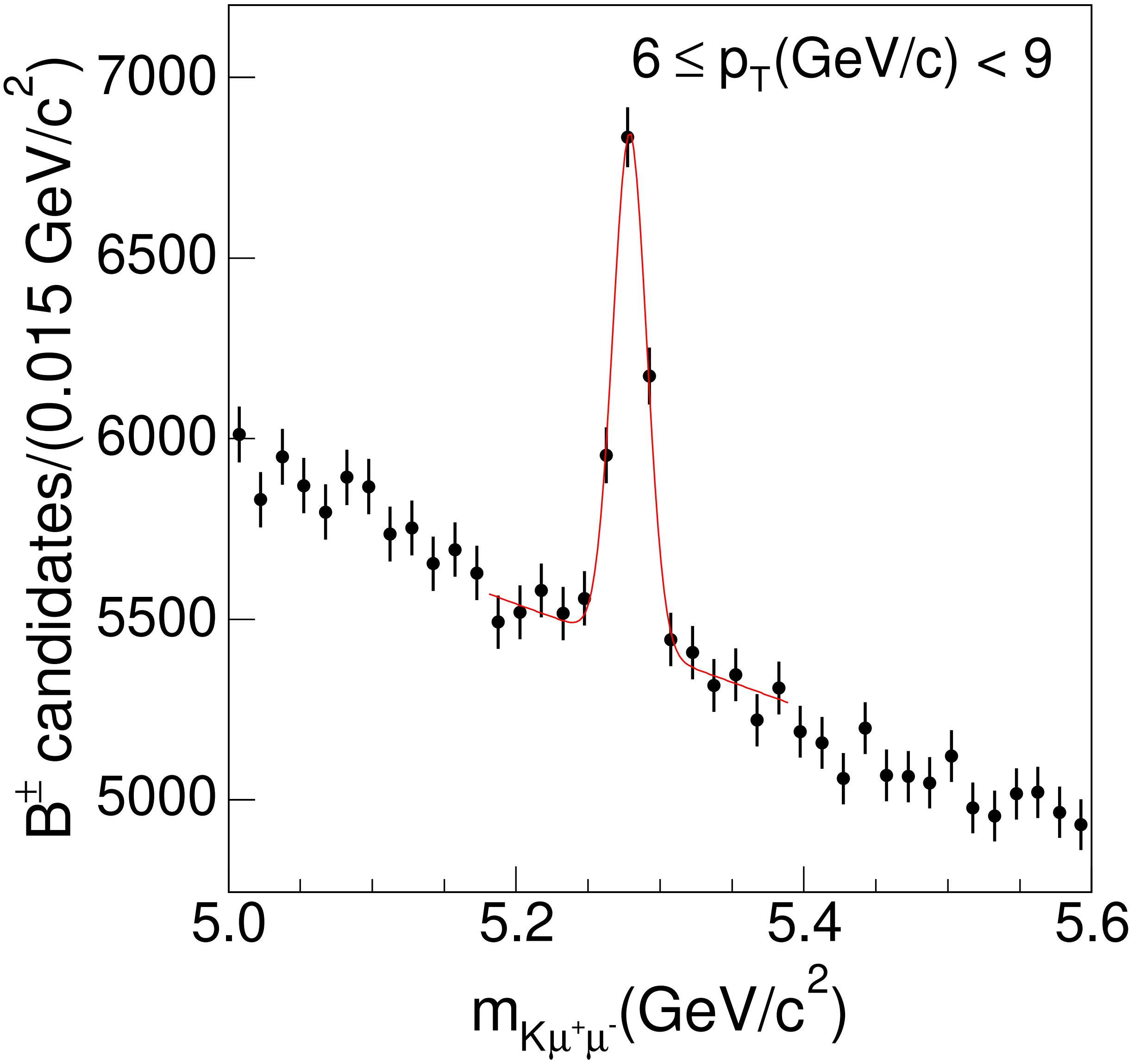

FIG. 2: Invariant mass distribution of $B^{\pm}$ candidates with $6 \leq p_T \leq 9$ GeV/c. The line represents the best fit to the data described in the text.

of L1 CMU trigger primitives. Simulated events are processed and selected with the same analysis code used for the data. The acceptances estimated using the simulation are listed in Table I. We use the data to verify the detector acceptance and efficiencies evaluated using the CDF II detector simulation. We adjust the simulation to match measurements in the data of: (1) the off-line COT track reconstruction efficiency; (2) the CMU detector

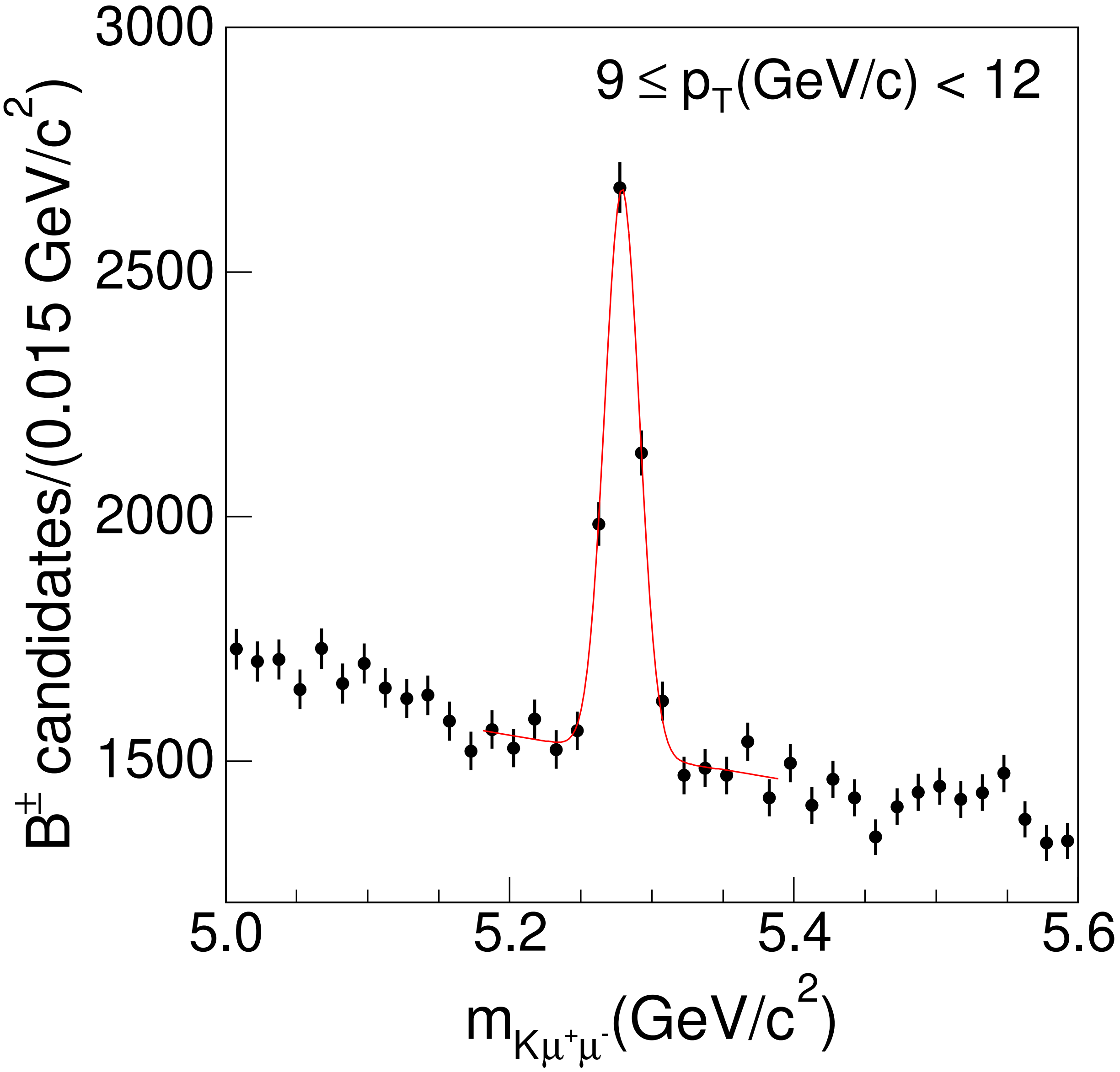

FIG. 3: Invariant mass distribution of $B^{\pm}$ candidates with $9 \leq p_T \leq 12$ GeV/c. The line represents the best fit to the data described in the text.

acceptance and efficiency; (3) the efficiency for finding L1 CMU primitives; and (4) the efficiency of the L1, L2, and L3 triggers.

In the simulation, the off-line COT track reconstruction efficiency is given by the fraction of tracks, which at generator level satisfy the p_T and η selection cuts, that survive after selecting fully simulated events as the data. The COT track reconstruction efficiency is found

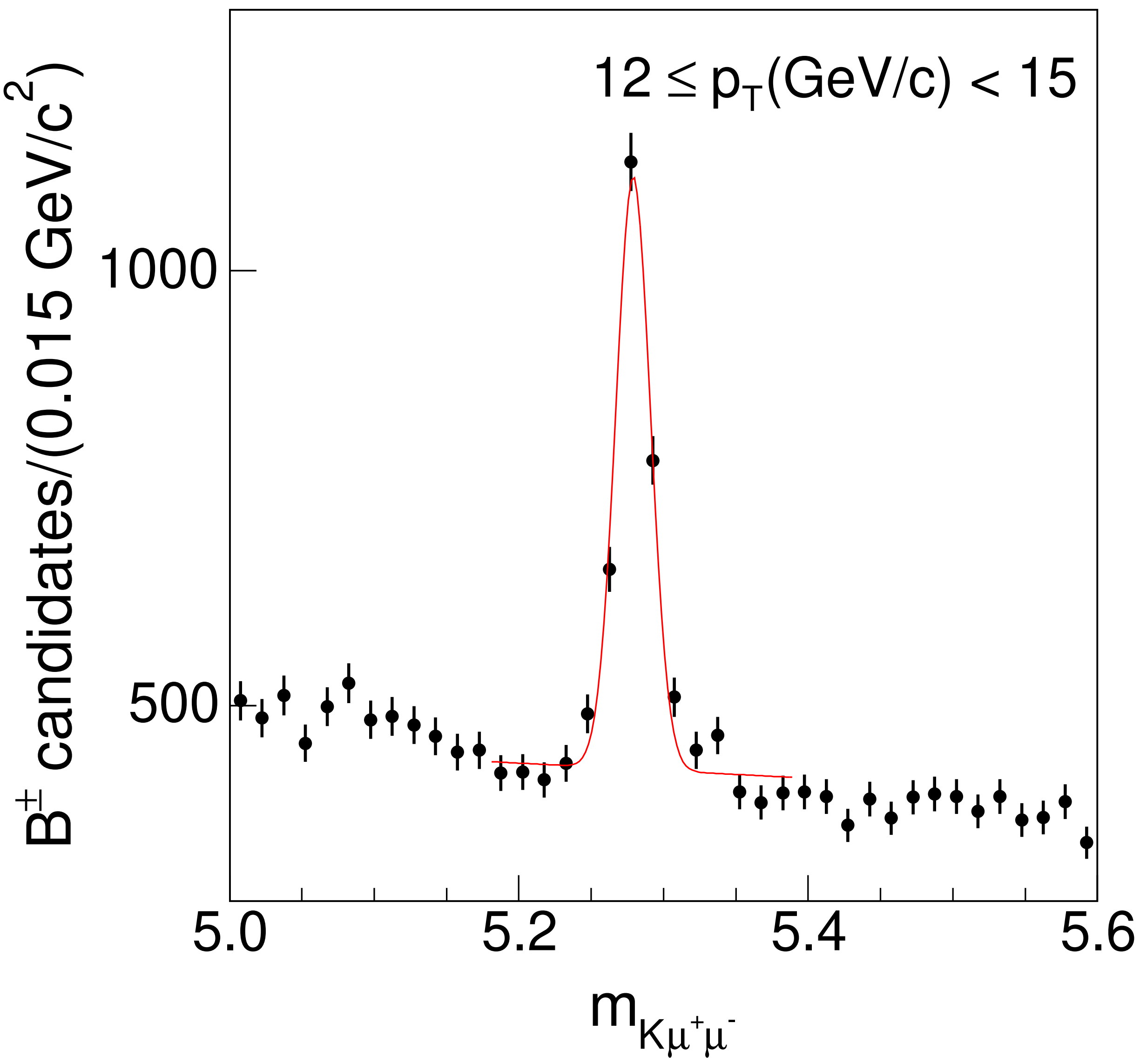

FIG. 4: Invariant mass distribution of $B^{\pm}$ candidates with $12 \leq p_T \leq 15$ GeV/c. The line represents the best fit to the data described in the text.

to be 0.998 ± 0.002. The same efficiency in the data is measured by embedding COT hits generated from simulated tracks into J/ψ data. In Ref. [30], the COT track reconstruction efficiency in the data is measured to be 0.996 with a $\simeq 0.006$ systematic accuracy [4]. We

[4] The efficiency measurement was performed in a subset of the data used for this analysis. Studies of independent data samples collected in the data taking period used for this analysis show that changes of

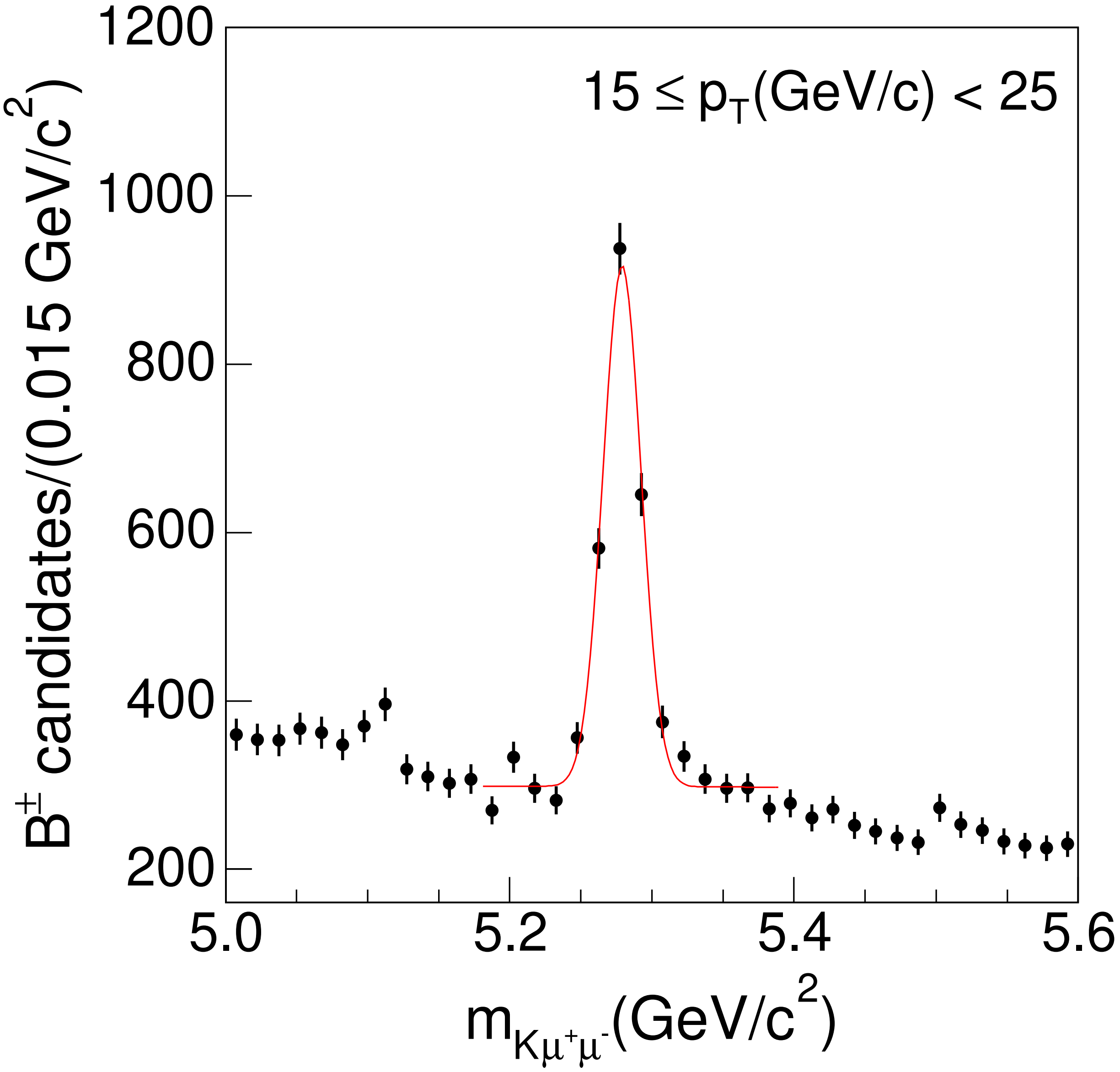

FIG. 5: Invariant mass distribution of $B^{\pm}$ candidates with $15 \leq p_T \leq 25$ GeV/c. The line represents the best fit to the data described in the text.

conclude that the efficiencies for reconstructing the μ^+ $\mu^- K^{\pm}$ system in the data and the simulation are equal within a 2% systematic error. Kaon decay and interactions are modeled with the CDF II detector simulation. Because of the uncertainties of the detector materials

the track reconstruction efficiency are appreciably smaller than the quoted systematic uncertainty [31].

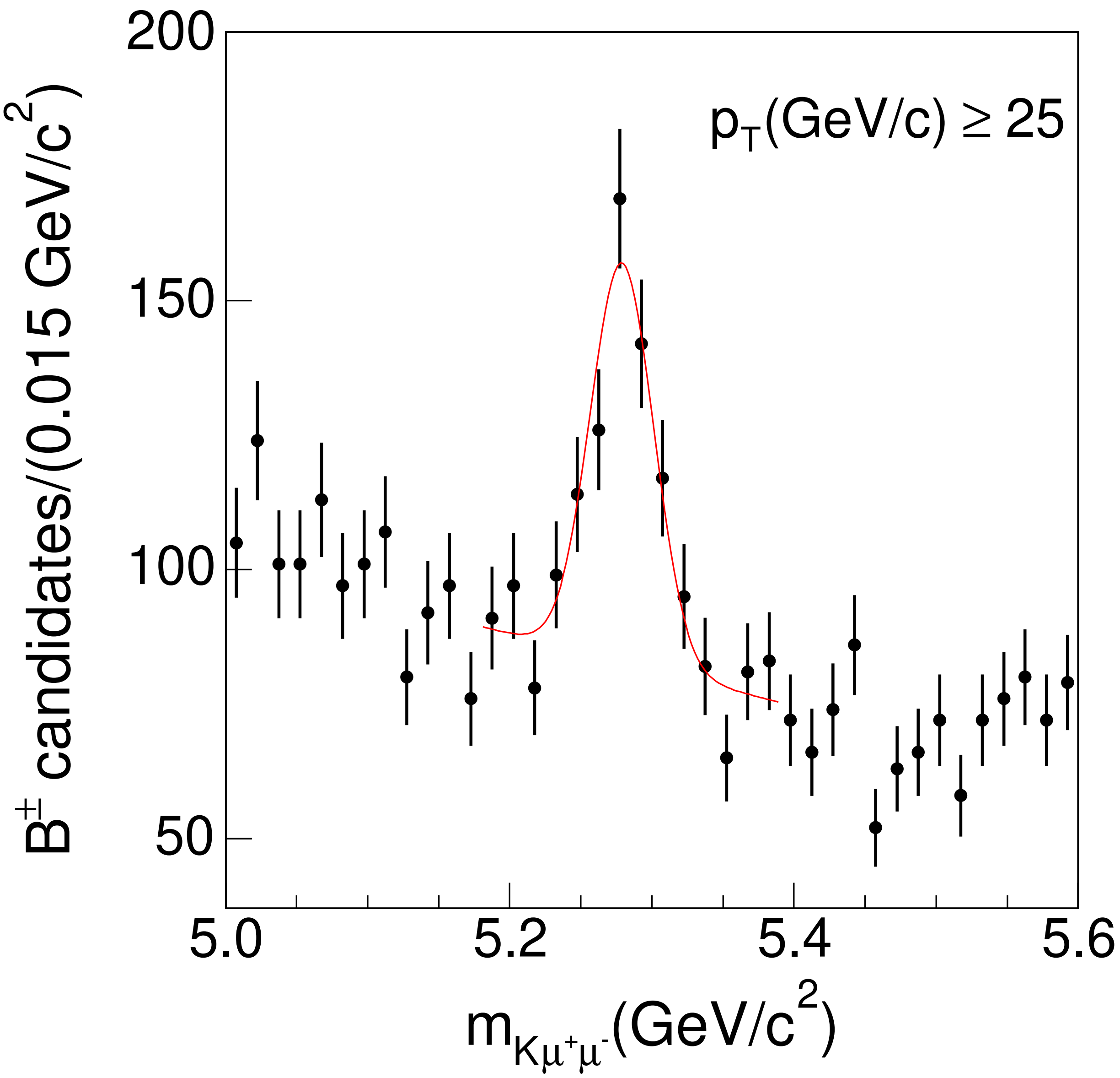

FIG. 6: Invariant mass distribution of $B^{\pm}$ candidates with $p_T \geq 25$ GeV/c. The line represents the best fit to the data described in the text.

and the nuclear interaction cross sections, the kaon tracking efficiency has an additional 0.3% uncertainty [32].

In the simulation, the fraction of CMU stubs generated by muon tracks with $p_T \geq 2$ GeV/c and $|\eta| \leq 0.8$ is 0.6439 ± 0.0004. In the data, this efficiency is measured by using $J/\psi \to \mu^+ \mu^-$ decays acquired with the μ-SVT trigger. We evaluate the invariant mass of all pairs of a CMUP track and a track with displaced impact parameter, $p_T \geq 2$ GeV/c, and $|\eta| \leq 0.8$. We fit the invariant mass distribution with a first order polynomial plus two Gaussian functions to extract the J/ψ signal. From the number of J/ψ mesons reconstructed using displaced tracks with or without a CMU stub (Fig. 7(a) and (b), respectively), we derive an efficiency of 0.6251 ± 0.0047. The integrated efficiency is evaluated after having weighted the p_T and η distributions of displaced tracks in the data to be equal to those of muons from B decays in the simulation.

In the simulation, the efficiency for finding a CMU primitive (CMU stub matched by a XFT track) is 0.8369 ± 0.0004. This efficiency is measured in the data by using events acquired with the CMUPp_T4 trigger. We combine the CMUP muon with all other CMU muons found in the event with and without a L1 CMU primitive. We extract the number of $J/\psi \to \mu^+\mu^-$ mesons by fitting the invariant mass distributions of all candidates with a first order polynomial plus two Gaussian functions. By comparing the fitted numbers of J/ψ candidates with and without L1 CMU primitive (Fig. 8(a) and (b), respectively) we derive an efficiency of 0.9276 ± 0.0005. The integrated efficiency is evaluated after having weighted the p_T and η distributions of the additional CMU muons to be equal to that of muons from B decays in the simulation.

In the simulation, the efficiencies of the L1 and L2 triggers are 0.9868 and 0.9939, respectively. By studying J/ψ candidates acquired with the CMUPp_T4 trigger, the L1 efficiency is measured to be 0.9879 ± 0.0009, and that of the L2 trigger 0.9948 ± 0.0001. The L3 trigger is not simulated. The L3 trigger efficiency is dominated by differences between the online and off-line reconstruction code efficiency [5]. The relative L3 efficiency for reconstructing a single muon identified by the off-line code has been measured to be 0.997 ± 0.002 [30]. The reconstruction efficiencies in the data and in the simulation are summarized in Table II.

B. Results

The differential cross section $d\sigma/dp_T$ is calculated as

$$\frac{d\sigma(B^+)}{dp_T} = \frac{N/2}{\Delta p_T \times \mathcal{L} \times \mathcal{A}_{\rm corr} \times BR} \tag{1}$$

[5] Online algorithms are faster but less accurate than the off-line reconstruction code.

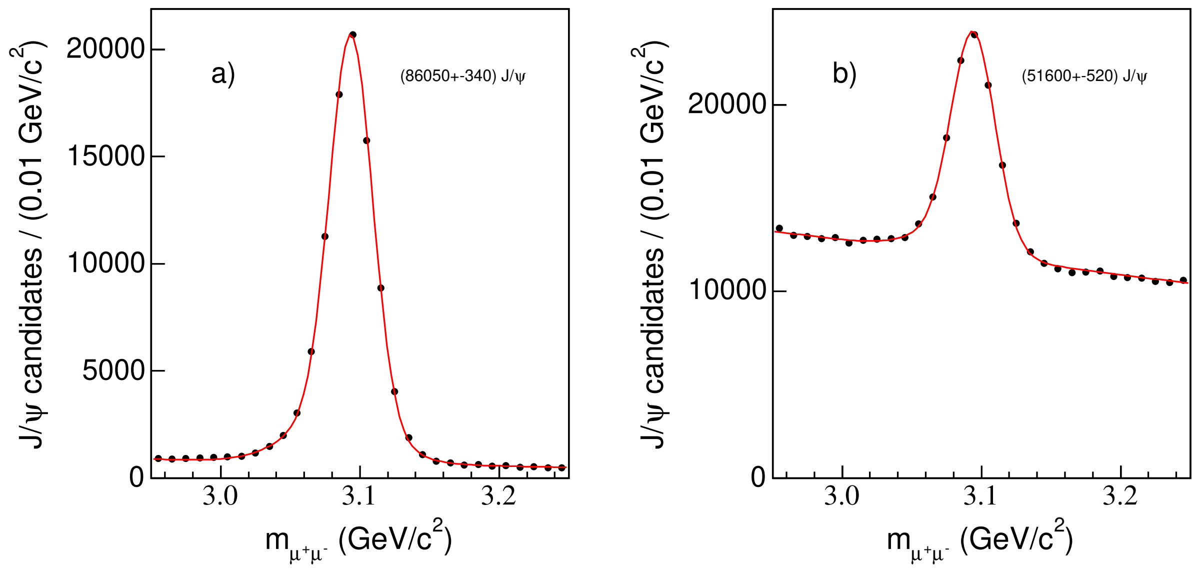

FIG. 7: Invariant mass distribution of a CMUP muon paired with all charged tracks in the event with (a) or without (b) a CMU stub.

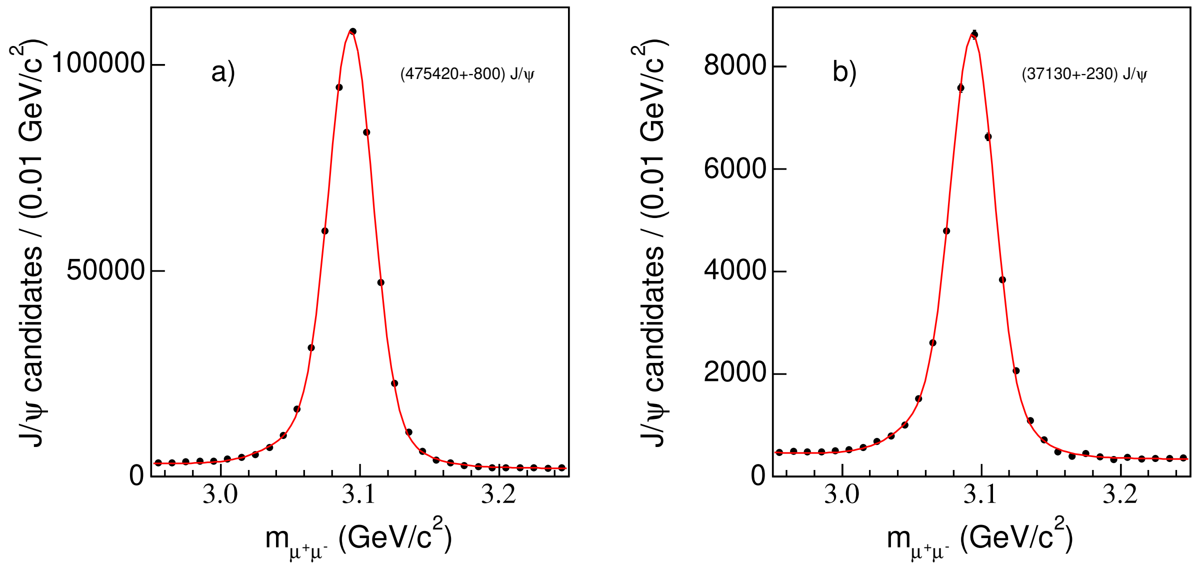

FIG. 8: Invariant mass distribution of a CMUP muon paired with all CMU muons in the event with (a) or without (b) a L1 CMU primitive.

TABLE II: Summary of efficiencies for reconstructing $B^{\pm}$ candidates in the data and the simulation. The last column indicates the corrections applied to the simulated acceptance and used to derive $\mathcal{A}_{\rm corr}$ in Table I.

Source	Data	Simulation	Corr.
COT tracking	$(0.996 \pm 0.006)^3$	$(0.998 \pm 0.002)^3$	1.00 ± 0.02
Kaon interaction			1.000 ± 0.003
CMU acc. and eff.	$(0.6251 \pm 0.0047)^2$	$(0.6439 \pm 0.0004)^2$	0.942 ± 0.014
L1 CMU primitives	$(0.9276 \pm 0.0005)^2$	$(0.8369 \pm 0.0004)^2$	1.228 ± 0.002
L1 eff.	0.9879 ± 0.0009	0.9868	1.0011 ± 0.0009
L2 eff.	0.9948 ± 0.0001	0.9939	1.0009 ± 0.0001
L3 eff.	$(0.997 \pm 0.002)^2$	1	0.994 ± 0.004
Total	0.328 ± 0.008	0.283 ± 0.002	1.152 ± 0.029

where N is the number of $B^{\pm}$ mesons determined from the likelihood fit to the invariant mass distribution of the $J/\psi\ K^{\pm}$ candidates in each p_T bin. The factor 1/2 accounts for the fact that both B^+ and B^- mesons are used and assumes C invariance at production. The bin width Δp_T and $\mathcal{A}_{\rm corr}$, the geometric and kinematic acceptance that includes trigger and tracking efficiencies measured with the data, are listed in Table I. The integrated luminosity of the data set is $\mathcal{L} = 739 \pm 44$ pb^{-1}. The branching ratio $BR = (5.98 \pm 0.22) \times 10^{-5}$ is derived from the branching fractions $BR(B^{\pm} \to J/\psi\ K^{\pm}) = (1.008 \pm 0.035) \times 10^{-3}$ and $BR(J/\psi \to \mu^+\ \mu^-) = (5.93 \pm 0.06) \times 10^{-2}$ [25].

The measured B^+ differential cross section as a function of its transverse momentum is listed in Table III . The integrated cross section is

$$\sigma_{B^+}(p_T \geq 6.0\ \text{GeV/c}, |y| < 1) = 2.78 \pm 0.24\ \mu\text{b}, \tag{2}$$

where the 8.8% error is the sum in quadrature of the 6% error on the integrated luminosity, the 3.6% uncertainty of the $B^+ \to J/\psi\ K^+$ and $J/\psi \to \mu^+\ \mu^-$ branching fractions, the 2.5% uncertainty of the acceptance calculation, the 2% systematic uncertainty of the fit, and the 4.4% statistical error.

For completeness, Figure 9 compares transverse momentum distributions in the data and

TABLE III: Observed differential cross section, $d\sigma/dp_T$ (nb/GeV/c), for B^+ mesons with rapidity $|y| \leq 1$. Errors are the sum in quadrature of statistical errors (shown in parentheses) and systematic errors due to luminosity (6%), branching ratios (3.6%), acceptance (2.5%), and fitting procedure (2.0%). Systematic errors are not p_T dependent. The integrated cross section for $p_T \geq 25$ GeV/c is 21.7 ± 3.7 nb.

$< p_T >$ (GeV/c)	Events	Acceptance (%)	$d\sigma/dp_T$
7.38	2792 ± 186	1.780 ± 0.045	591.7 ± 59.0 (39.3 stat.)
10.38	2373 ± 110	4.405 ± 0.111	203.2 ± 17.8 (9.4 stat.)
13.39	1365 ± 66	6.872 ± 0.173	74.9 ± 6.6 (3.6 stat.)
19.10	1390 ± 63	10.16 ± 0.25	15.5 ± 1.3 (0.7 stat.)
≥ 25	277 ± 44	14.42 ± 0.36	

in the simulation, based on the NLO QCD prediction [2], that has been used to evaluate the detector acceptance. Data and simulation are normalized to the same number of events. Each distribution is constructed using $J/\psi K^\pm$ candidates with invariant mass in the range $5.255 - 5.315$ GeV/c^2 (region #1). The background contribution is subtracted using candidates in the mass range $5.18 - 5.24$ and $5.33 - 5.425$ GeV/c^2. The background normalization is the number of events in region #1 minus the number of $B^\pm$ candidates determined by the fit listed in Table III. One notes the fair agreement between data and untuned QCD prediction [6].

V. CONCLUSIONS

We use the exclusive decay $B^\pm \to J/\psi\ K^\pm$ to measure the B^+ production cross section in $p\bar{p}$ collisions at $\sqrt{s} = 1960$ GeV. The measurement is based on a sample of 8197 ± 239 $B^\pm$ mesons selected from 739 pb^{-1} of data collected with the CDF II detector at the Fermilab

[6] The p_T distributions of the $B^\pm$ and J/ψ mesons in the data are slightly softer than those of the simulation; this difference is not relevant for the result of the study because the $B^\pm$ kinematic acceptance has been evaluated for each p_T^B-bin and the calibration of the simulated acceptance using the data do not depend on the muon and kaon transverse momenta.

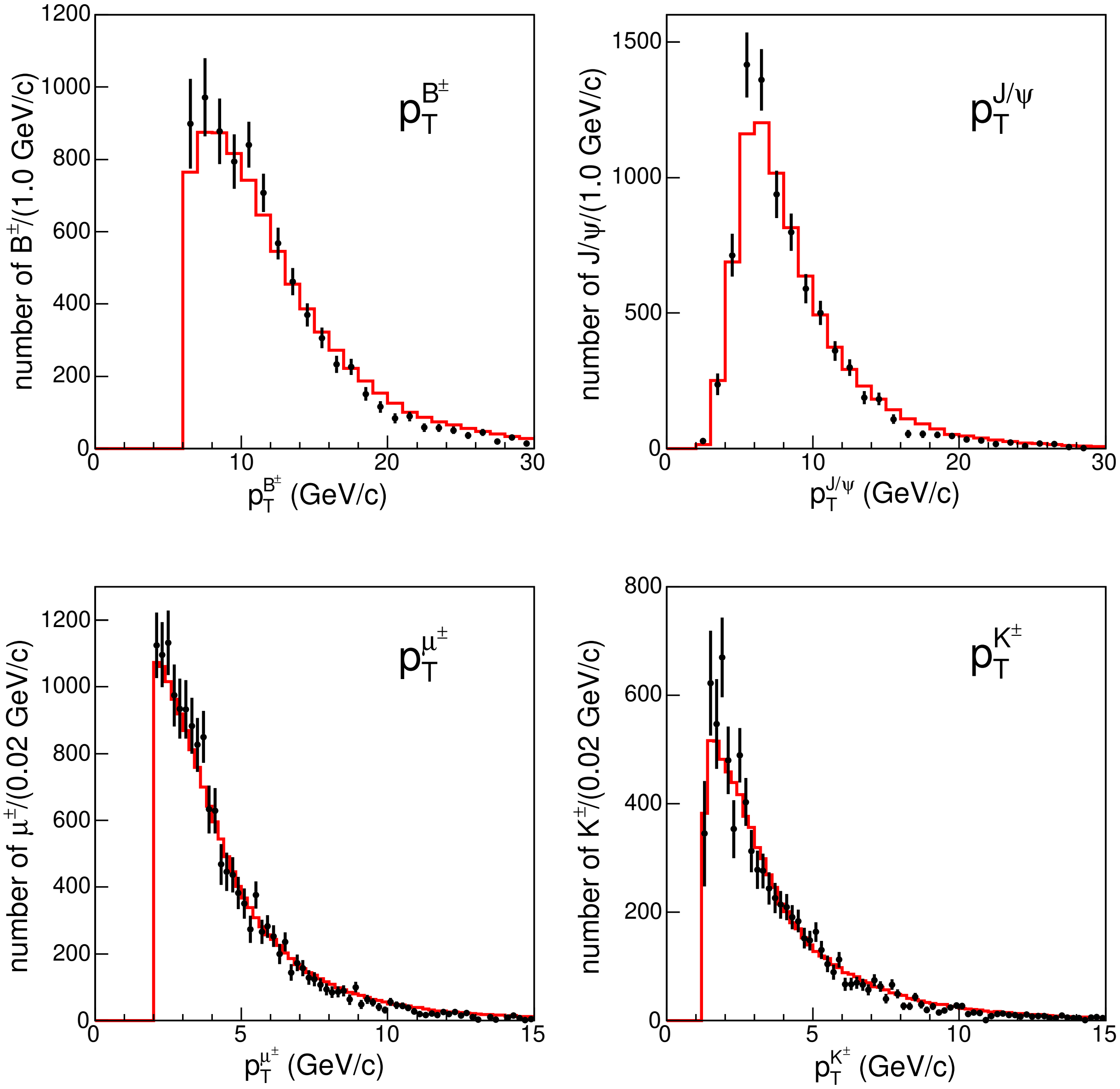

FIG. 9: Transverse momentum distributions in the data ($\bullet$) and simulation (solid histogram). The simulation is normalized to the $B^{\pm} \to \mu^+\,\mu^-\,K^{\pm}$ signal observed in the data (see text).

Tevatron collider. The B^+ production cross section is measured to be

$$\sigma_{B+}(p_T \geq 6.0 \;\; \mathrm{GeV/c}, |y| < 1) = (2.78 \pm 0.24)\;\mu\mathrm{b}.$$

To compare with other Tevatron measurements, we choose as a theoretical benchmark the NLO QCD prediction [1] that uses a b-quark mass of $m_b = 4.75$ GeV/c^2, renormalization and factorization scales $\mu_R = \mu_F = \sqrt{p_T^2 + m_b^2}$, the MRSD$_0$ [6] fit to the parton distribution functions (PDF), a fragmentation fraction $f_u = 0.375$, and a fragmentation model based on the Peterson fragmentation function with the ϵ parameter set to 0.006. The ratio of the present measurement to this theoretical prediction is 2.80 ± 0.24. Previous measurements of the single b-quark cross section based on the detection of J/ψ mesons yield the following ratios to the same theoretical prediction: 2.9 ± 0.67 [9], 4.0 ± 0.6 [10], 4.0 ± 0.4 [33], and 3.14 ± 0.28 [30]. In contrast, all CDF and DØ measurements of the single b production cross section that are based upon detection of a lepton from b-quark decays [11–15] yield a smaller average ratio to the same theoretical prediction (2.2 with a 0.2 RMS deviation [5]). As shown in Fig 10, our measurement agrees with the value inferred from the J/ψ inclusive cross section [30] [$\sigma_{B^+}(p_T \geq 6.0 \text{ GeV/c}, |y| < 1) = 2.4 \pm 0.4\ \mu$b] and is within the range of values predicted by the FONLL QCD calculation [2, 34] that uses $f_u = 0.389$ [25] and the CTEQ6M fits to the parton distribution functions [35] (2.1 μb with a $\simeq 30\%$ theoretical uncertainty [4]).

VI. ACKNOWLEDGMENTS

We thank the Fermilab staff and the technical staffs of the participating institutions for their vital contributions. This work was supported by the U.S. Department of Energy and National Science Foundation; the Italian Istituto Nazionale di Fisica Nucleare; the Ministry of Education, Culture, Sports, Science and Technology of Japan; the Natural Sciences and Engineering Research Council of Canada; the National Science Council of the Republic of China; the Swiss National Science Foundation; the A.P. Sloan Foundation; the Bundesministerium für Bildung und Forschung, Germany; the Korean Science and Engineering Foundation and the Korean Research Foundation; the Particle Physics and Astronomy Research Council and the Royal Society, UK; the Institut National de Physique Nucleaire et Physique des Particules/CNRS; the Russian Foundation for Basic Research; the Comisión Interministerial de Ciencia y Tecnología, Spain; the European Community's Human Potential Programme under contract HPRN-CT-2002-00292; and the Academy of Finland.

[1] P. Nason, S. Dawson and R. K. Ellis, Nucl. Phys. **B327**, 49 (1989); Erratum-ibid. **B335**, 260 (1990). W. Beenakker *et al.,* Nucl. Phys. **B351**, 507 (1991).

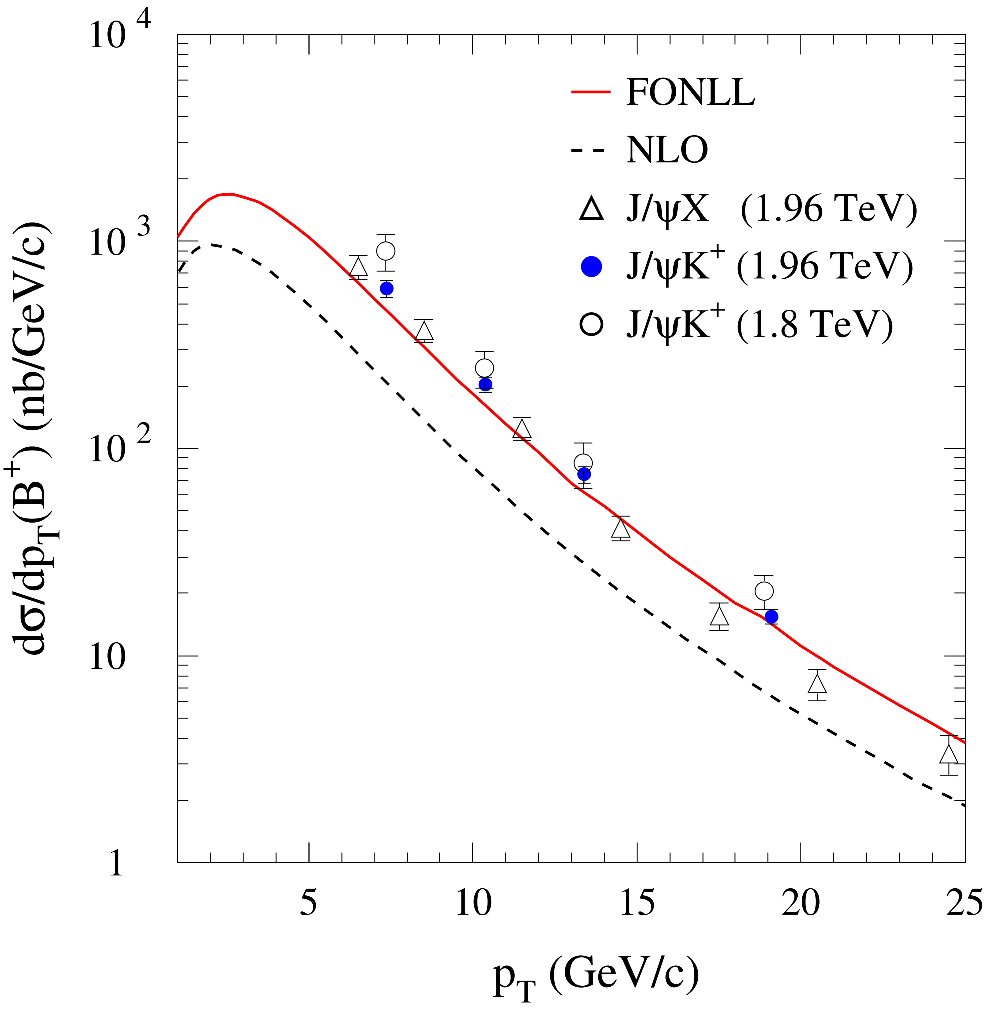

FIG. 10: Measurements of the B^+ differential cross section ($|y^{B^+}| \leq 1$) at the Tevatron are compared to the NLO and FONLL theoretical predictions (see text). The result of this experiment ($\bullet$) is shown together with those of ($\triangle$) Ref. [30] and ($\circ$) Ref. [9]; the result of Ref. [9] has been increased by 10% to account for the expected increase of the cross section from $\sqrt{s} = 1.8$ to 1.96 TeV [1].

[2] M. Cacciari *et al.,* JHEP **9805**, 007 (1998).

[3] S. Frixione *et al.* Adv. Ser. Direct. High Energy Phys. **15**, 609 (1998) [arXiv:hep-ph/9702287].

[4] M. Cacciari *et al.,* JHEP **0407**, 033 (2004).

[5] F. Happacher *et al.,* Phys. Rev. D **73**, 014026 (2006); F. Happacher, *Status of the Observed and Predicted $b\bar{b}$ Cross Section at the Tevatron*, `www-conf.kek.jp/dis06/doc/WG5/hfl20-happacher.ps`, to appear in the Proceedings of DIS 2006, Tsukuba, Japan.

[6] A. D. Martin, W. J. Stirling and R. G. Roberts, Phys. Rev. D **47**, 867 (1993).

[7] C. Peterson *et al.,* Phys. Rev. D **27**, 105 (1983).

[8] J. Chrin, Z. Phys. **C36**, 163 (1987).

[9] F. Abe *et al.,* Phys. Rev. Lett. **75**, 1451 (1995).

[10] D. Acosta *et al.,* Phys. Rev. D **65**, 052005 (2002).

[11] F. Abe *et al.,* Phys. Rev. Lett. **71**, 2396 (1993).

[12] F. Abe *et al.,* Phys. Rev. Lett. **71**, 500 (1993).

[13] S. Abachi *et al.,* Phys. Rev. Lett.**74**, 3548 (1995).

[14] B. Abbott *et al.,* Phys. Lett. B **487**, 264 (2000).

[15] B. Abbott *et al.,* Phys. Rev. Lett. **85**, 5068 (2000).

[16] F. Abe *et al.,* Nucl. Instrum. Methods. Phys. Res., Sect. A **271**, 387 (1988).

[17] R. Blair *et al.,* Fermilab Report No. FERMILAB-Pub-96/390-E, 1996.

[18] A. Sill *et al.,* Nucl. Instrum. Methods. Phys. Res., Sect. A **447**, 1 (2000).

[19] T. Affolder *et al.,* Nucl. Instrum. Methods. Phys. Res., Sect. A **526**, 249 (2004).

[20] G. Ascoli *et al.,* Nucl. Instrum. Methods. Phys. Res., Sect. A **268**, 33 (1988).

[21] J. Elias *et al.,* Nucl. Instrum. Methods. Phys. Res., Sect. A **441**, 336 (2000).

[22] D. Acosta *et al.,* Nucl. Instrum. Methods. Phys. Res., Sect. A **461**, 540 (2001).

[23] M. M. Block and R. N. Cahn, Rev. Mod. Phys. **57**, 563 (1985).

[24] S. Klimenko *et al.,* Fermilab Report No. FERMILAB-FN-0741, 2003.

[25] W. M. Yao *et al.,* J. Phys. Lett. **633**, 1 (2006).

[26] A. Abulencia *et al.,* *Measurement of the Branching Fractions* $BR(B^{\pm} \to J/\psi\, \pi^{\pm})/BR(B^{\pm} \to J/\psi\, K^{\pm})$, to be submitted to Phys. Rev. D.

[27] D. J. Lange, Nucl. Instrum. Meth. A **462**, 152 (2001).

[28] B. Aubert *et al.,* Phys. Rev. D **65**, 032001 (2002).

[29] R. Brun *et al.,* CERN Report No. CERN-DD-78-2-REV; R. Brun *et al.,* CERN Programming

Library Long Write-up W5013 (1993).

[30] D. Acosta *et al.,* Phys. Rev. D **71**, 032001 (2005).

[31] A. Abulencia *et al.,* Phys. Rev. Lett. **95**, 252001 (2005).

[32] D. Acosta *et al.,* Phys. Rev. Lett. **94**, 122001 (2005).

[33] F. Abe *et al.,* Phys. Rev. Lett. **79**, 572 (1997).

[34] M. Cacciari and P. Nason, Phys. Rev. Lett **89**, 122003 (2002).

[35] J. Pumplin *et al.,* JHEP **0207**, 012 (2002).